Journal of Applied Mechanics and Technical Physics, Vol. 51, No. 1, pp. 65–73, 2010

AERODYNAMIC CHARACTERISTICS OF A BODY OF REVOLUTION WITH GAS-PERMEABLE SURFACE AREAS

V. M. Fomin,[1] V. I. Zapryagaev,[1] A. V. Lokotko,[1]
V. F. Volkov,[1] A. E. Lutskii,[2] I. S. Men'shov,[2]
Yu. M. Maksimov,[3] and A. I. Kirdyashkin[3]

UDC 533.6.013.125

Results of experimental studies and numerical calculations of aerodynamic characteristics of a supersonic flow around a body of revolution with a gas-permeable porous nose cone and an internal duct are presented. At a flow velocity corresponding to the Mach number M = 3*, the body considered is found to have a lower drag coefficient (approximately by* 9%*) than a similar body impermeable for the gas and a lower streamwise static stability.*

Key words: *cone–cylinder body of revolution, supersonic flow velocity, drag coefficient, gas-permeable porous surface, streamwise stability, aerodynamic tests.*

Introduction. The use of permeable porous materials (PPMs) offers new possibilities of flow control on elements of flying vehicles designed for motion at high supersonic velocities in dense atmospheric layers. In particular, PPMs can be used on transonic airfoils to reduce the intensity of the closing shock wave and to eliminate separation induced by this shock wave [1]. Redistribution (with the use of PPMs) of the high pressure from the lower to the upper wing surface makes it possible to prevent a drastic decrease in the lift force at high angles of attack, while the permeable nose part allows the vehicle motion to be made more stable in terms of the angles of rolling and yawing. Hartman and Morgenstern [2] assumed that the use of a gas-permeable nose part in a supersonic aircraft contributes to reduction of the sonic boom level. Zaikovskii et al. [3] demonstrated that the use of PPM inserts in rocket motor nozzles allows their thrust in the overexpansion mode of operation to be increased by 2–3%. In rocket engineering, PPMs are widely used for thermal protection [4].

According to [5], the base drag caused by rarefaction in the base wake in the atmospheric flight with supersonic velocities can reach 40% of the frontal drag. It is known that injection of a small amount of a gas (1–2% of the incoming mass flow in the mid-section) to the base region makes it possible to substantially increase the base pressure and, hence, reduce the base drag [5–8]. A source of the additional gas mass can be atmospheric air redistributed over internal ducts from the elevated pressure region on the frontal part of the body to the base region [9]. Nevertheless, shock waves arising on the edges of the orifices or slots in the frontal part of the body induce an additional wave drag and eliminate the effect of the base pressure increase.

An additional study of the above-mentioned method of base drag reduction, which was proposed in [9], was stimulated by the development of new PPMs obtained by methods of powder metallurgy [10]. It was assumed that inserts made of these materials and installed in the frontal and rear parts of the body of revolution can ensure a necessary mass flow of air for its transfer to the base region, but do not generate an additional wave drag because small pores are submerged into the subsonic region of the boundary layer.

[1]Khristianovich Institute of Theoretical and Applied Mechanics, Siberian Division, Russian Academy of Sciences, Novosibirsk 630090; lok@itam.nsc.ru. [2]Keldysh Institute of Applied Mathematics, Russian Academy of Sciences, Moscow 125047. [3]Department of Structural Macrokinetics, Tomsk Research Center, Siberian Division, Russian Academy of Sciences, Tomsk 634021. Translated from Prikladnaya Mekhanika i Tekhnicheskaya Fizika, Vol. 51, No. 1, pp. 79–88, January–February, 2010. Original article submitted February 26, 2009.

0021-8944/10/5101-0065 © 2010 Springer Science + Business Media, Inc.

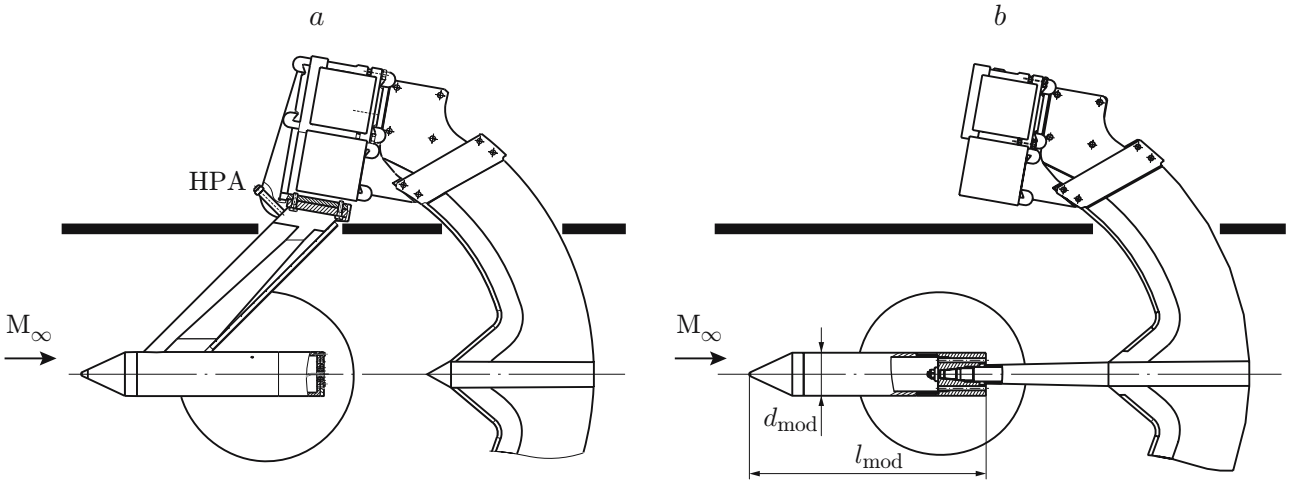

Fig. 1. Model mounting in the wind-tunnel test section: (a) on a side strut; (b) on a central base sting; HPA means the high-pressure air.

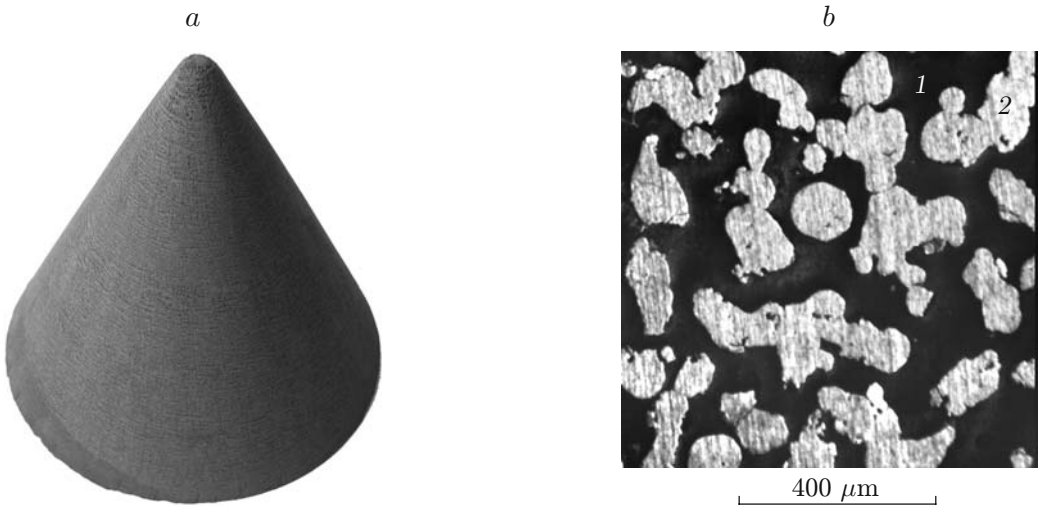

Fig. 2. Gas-permeable porous cone: (a) general view; (b) sectional view; 1) channels for gas transportation; 2) drops of the Ni–Cr–Al alloy.

The present paper describes the results of experimental and numerical investigations of this method of base drag reduction and associated changes in other aerodynamic characteristics.

Experimental Technique. The experiments were performed in a T-313 supersonic wind tunnel based at the Khristianovich Institute of Theoretical and Applied Mechanics, Siberian Division, Russian Academy of Sciences. The wind-tunnel test section is $0.6 \times 0.6 \times 2.0$ m. The experiments were performed at Mach numbers M = 3.02 and 4.03; the corresponding Reynolds numbers were $\text{Re} = 3.55 \cdot 10^7$ and $4.86 \cdot 10^7$ m^{-1}, respectively.

Two models of a blunted cone–cylinder body of revolution were considered (Fig. 1). The cylinder diameter was $d_{\text{mod}} = 100$ mm and the model lengths were $l_{\text{mod}} = 550$ mm (long model) and 230 mm (short model). The apex half-angle of the cone was $\beta = 25°$, and the relative bluntness was $r^0 = r_k/d_{\text{mod}} = 0.1$. Two replaceable cones were used: a smooth impermeable cone with the surface roughness approximately equal to 1.6 μm and a permeable porous cone (Fig. 2a) fabricated by the method of self-propagating high-temperature synthesis [10]. The structure of the permeable porous cone was a system of connected metallic microdrops with a rounded shape and variable-section channels for gas transportation (Fig. 2b). The material porosity was approximately 60%, and the mean channel size was 100 μm. The configuration of the porous cone reproduced the configuration of the impermeable cone. The base surface of the model had holes, and the permeability having the maximum value $S_{\text{hole}}/S_{\text{mid}} = 18\%$ could be changed by rotating an adjacent disk with holes.

The model had an inner cavity reaching the base surface. The cavity in the long model ($l_{\text{mod}} = 550$ mm) was a duct where a hot-wire flow meter was located.

The long model could be fixed in the test section by two methods: 1) on a side strut (Fig. 1a); 2) on a base sting (Fig. 1b). The strut had a channel for injection of air from a high-pressure pipeline into the model. The high-pressure air pipeline was equipped with a standard flow meter and was uncoupled at the points of its attachment to the weighted elements (the force influence was eliminated). Forced injection of air with a controlled mass flow to the base face of the model with an impermeable nose cone made it possible to determine the drag coefficient c_x and compare it with available data. The air mass flow corresponding to the minimum value of c_x was normalized to the air mass flow through the porous cone for the wind-tunnel test conditions, and the required mass flow characteristics of the permeable cone were specified on this basis.

The parameters measured on the long model were the air mass flow in the duct and the base pressure.

The short model ($l_{\text{mod}} = 230$ mm) was fixed only on the base sting, and there was no forced injection of air into the model. In all cases, the aerodynamic characteristics of the model were determined by weighting the model on an external aerodynamic balance.

On the short model, we determined the characteristics of the streamwise stability and visualized the flow in the vicinity of the nose cone with the use of a Videoscan 285/P camera and an IAB-451 shadowgraph.

Comparative tests of the model with a smooth impermeable cone and a permeable porous cone in the wind tunnel without external supply of air into the model allowed us to study the effect of the porous cone on the aerodynamic characteristics of the model.

The drag coefficients of the model with gas-permeable inserts were normalized to the drag coefficient c_{x0} of the long model with the impermeable nose cone; the influence of the strut and the base sting was eliminated. In calculating the coefficient c_x, the value of c_{x0} was used as a basic value, and the mid-section area was used as a reference area.

The value of the coefficient c_{x0} was determined by using a variant of the method of "doubling" on the basis of results of three tests:

$$c_{x0} = (c_{pb})_1 + (c_x)_2 + (c_x)_{\text{flow}}.$$

Here, $(c_{pb})_1 = (p_b - p_\infty)/q$ is the base pressure coefficient determined in tests by variant No. 1 (Fig. 1a), $(c_x)_2$ is the drag coefficient of the model determined in tests by variant No. 2 (Fig. 1b) where the base drag was eliminated (p_b is the base pressure, p_∞ is the pressure in the test section of the wind tunnel and $q = \varkappa p_\infty \mathrm{M}^2/2$ is the dynamic pressure), and $(c_x)_{\text{flow}}$ is the "flow" coefficient characterizing the effect of the base sting and obtained with the use of a special "non-balance" model with a controlled duct flow [11].

The value obtained in the experiment is $(c_{x0})_{\text{exp}} = 0.5329$; the value of this coefficient calculated at the Keldysh Institute of Applied Mathematics, Russian Academy of Sciences for a body with the configuration of the examined model under flight conditions in an undisturbed atmosphere at Mach and Reynolds numbers corresponding to the experimental conditions is $(c_{x0})_{\text{calc}} = 0.5326$. Thus, the difference between the experimental and numerical data is smaller than 0.05%. The value $c_{x0} = 0.5329$ was taken as a basic value.

Experiments with an Impermeable Nose Cone and Forced Injection of Air into the Base Region. The experiments were performed on a model fixed on the side strut with completely opened base perforation. We studied the relative base pressure $\bar{p} = p_b/p_\infty$ and the drag coefficient as functions of the relative mass flow of the injected gas $\bar{G} = G_0/(\rho_\infty U_\infty S_{\text{mid}})$ (ρ_∞ and U_∞ are the free-stream density and velocity; S_{mid} is the mid-section area of the model). The dependences of $\bar{p}$ and c_x on $\bar{G}$ are plotted in Fig. 3. It is seen that $\bar{p} = 0.44$ in the case without forced injection. It was shown [5, 8] that the base pressure depends on the Reynolds number based on the model length Re_l. In the case considered, we have $\mathrm{Re}_l \approx 2 \cdot 10^7$, and the results obtained for M = 3 are in good agreement with the known values for rotating missiles [12]. At the relative mass flow of air $\bar{G} = 2.4\%$, we obtained the maximum value of the relative pressure $\bar{p} = 0.787$, which is higher than the value of $\bar{p}$ in the absence of injection by 55%. The value $\bar{G} = 2.4\%$ is close to the available data for the maximum value of $\bar{p}$ in the case of gas injection into the base wake behind a body of revolution in a flow with a Mach number M = 3, but the maximum value depends on the degree of permeability of the base surface [5].

In the case of air injection into the base region, the drag coefficient c_x decreases (see Fig. 3). At the relative mass flow of air $\bar{G} \approx 2.4\%$, the drag coefficient c_x reaches the first minimum with respect to the value of c_x in the absence of injection; the change is $\Delta c_x = -0.0619$, which is $\delta c_x = 11.6\%$ with respect to the basic value. A further decrease in c_x with increasing $\bar{G}$ is determined by the momentum of the exhausting jet.

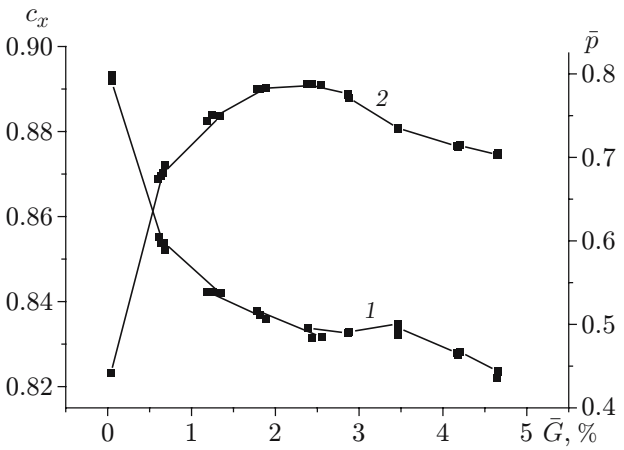

Fig. 3. Drag coefficient c_x (curve 1) and relative base pressure $\bar{p}$ (curve 2) of the model with a smooth impermeable cone versus the relative mass flow of air $\bar{G}$ with external injection to the base region (M = 3.02).

Thus, the relative mass flow for air injection $\bar{G}$ = 2.0–2.4% is the optimal value for reducing the drag coefficient c_x in the case of a passive flow through the body, which agrees with the data of [5].

Effect of the Nose Cone Type on the Aerodynamic Characteristics. The effect of the smooth impermeable cone and the gas-permeable nose cone on the drag coefficient c_x was studied on a model mounted on the side strut (see Fig. 1a) without external injection. The air flow through the gas-permeable cone and the model body was controlled by opening or closing base holes. The tests were performed at angles of attack $\alpha = \pm(0\text{–}2)^\circ$.

The greatest drag coefficient $c_x = 0.8875$ at $\alpha = 0^\circ$ was obtained for the model with the smooth impermeable cone (Fig. 4).

In the model with the permeable cone and without the duct flow through the model body to the base region at the same angle of attack ($\alpha = 0^\circ$), the drag coefficient decreases to $c_x = 0.8778$ ($\Delta c_x = -0.0097$ and $\delta c_x = 1.82\%$).

Zakharchenko and Kardanov [8] noted that installation of porous nose cones at Reynolds numbers close to the values corresponding to the boundary-layer transition from the laminar to the turbulent state leads to flow turbulization, which results in an increase in base pressure. Figure 5 shows the relative base pressures obtained in experiments. It is seen that the pressures on the models with smooth and porous cones without the duct flow almost coincide.

Thus, the effect observed is apparently caused by redistribution of pressure on the head part of the model owing to air overflow inside the porous cone from the region behind the normal shock in the vicinity of the cone apex toward the cone base, to the region under the cone shock. A possible consequence is the change in the effective shape of the head part of the model and reduction of drag, which was also noted in [4, 8].

The results of numerical calculations of the flow for this case are plotted in Figs. 6 and 7. The directions of the velocity vectors confirm the assumption about the internal overflow in the model cavity and the opposing exhaustion of air near the cone base in the region $r/r_{\text{mod}} = 0.8\text{–}1.0$. The results are the displacement of the incoming flow, a decrease in pressure in this region (see Fig. 7), and a decrease in the frontal drag.

The presence of a duct flow through the model with a permeable nose cone with a relative mass flow $\bar{G} = 1.15\%$ leads to a substantial decrease in the drag coefficient to $c_x|_{\alpha=0} = 0.8380$. The value $\bar{G} = 1.15\%$ is smaller than the optimal value obtained above for the case with forced injection (see Fig. 3); it was determined by the permeability of the porous cone. As compared with an impermeable cone, the increment is $\Delta c_x = -0.0494$; with respect to the basic value c_{x0}, the increment is $\delta c_x = 9.3\%$. The main contribution to the decrease in the coefficient c_x is made by the increase in the base pressure (see Fig. 5); the decrease in pressure on the nose cone surface exerts a much smaller effect (see Fig. 7).

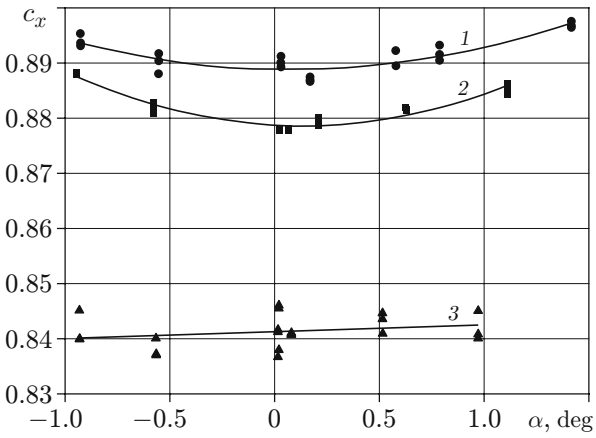

Fig. 4

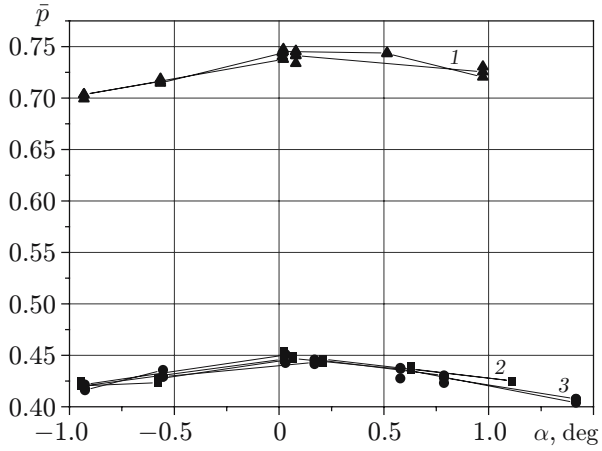

Fig. 5

Fig. 4. Drag coefficient c_x of the model with different nose cones versus the angle of attack α in the case of passive flow and M = 3.02: 1) smooth impermeable nose cone; 2) porous cone without duct flow through the model; 3) porous cone with duct flow through the model body.

Fig. 5. Relative base pressure $\bar{p}$ versus the angle of attack α in the model with different nose cones in a flow with a Mach number M = 3.02: 1) porous cone ($\bar{G} = 1.15\%$); 2) porous cone without duct flow; 3) smooth impermeable cone.

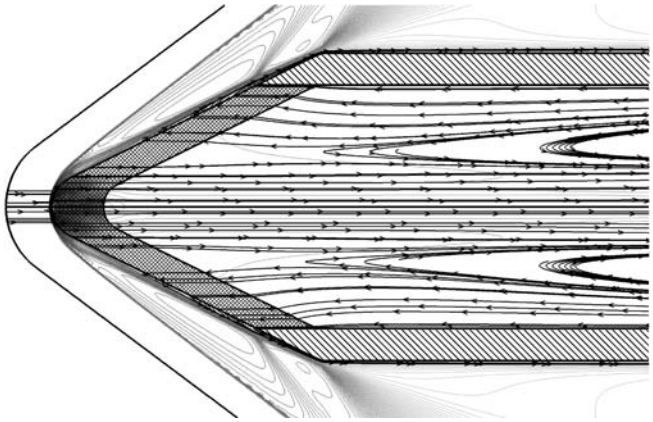

Fig. 6

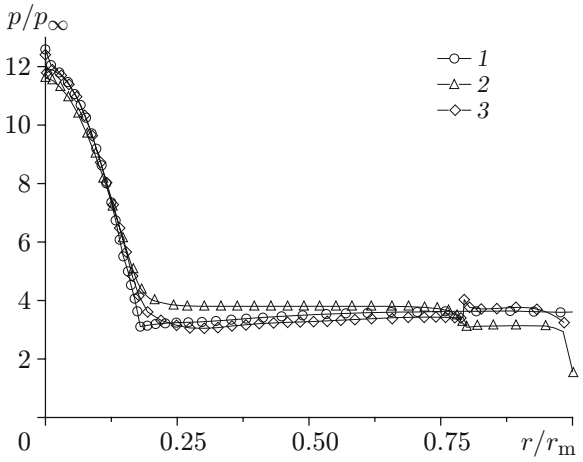

Fig. 7

Fig. 6. Numerical calculation of the external flow around a porous nose cone and the flow in the inner cavity of the model in a flow with M = 3.02: the arrows indicate the directions of the velocity vectors.

Fig. 7. Pressure distribution on the nose cone surface in a flow with M = 3.02: 1) smooth impermeable cone; 2) porous cone without duct flow; 3) porous cone with duct flow.

It seems of interest to study the dependence of the coefficient c_x on the angle of attack α for different variants of the model (see Fig. 4). If there is no duct flow (curves 1 and 2 in Fig. 4), the dependences have a clearly expressed parabolic shape with a minimum of c_x in the vicinity of $\alpha = 0°$. In the presence of the duct flow (curve 3), the angle of attack in the examined range exerts a minor effect on the drag coefficient. The reason is the change in the pressure distribution pattern behind the shock waves on the porous nose cone, as compared with the impermeable nose cone at different angles of attack. This phenomenon can affect the characteristics of the streamwise stability, which was also noted in [4].

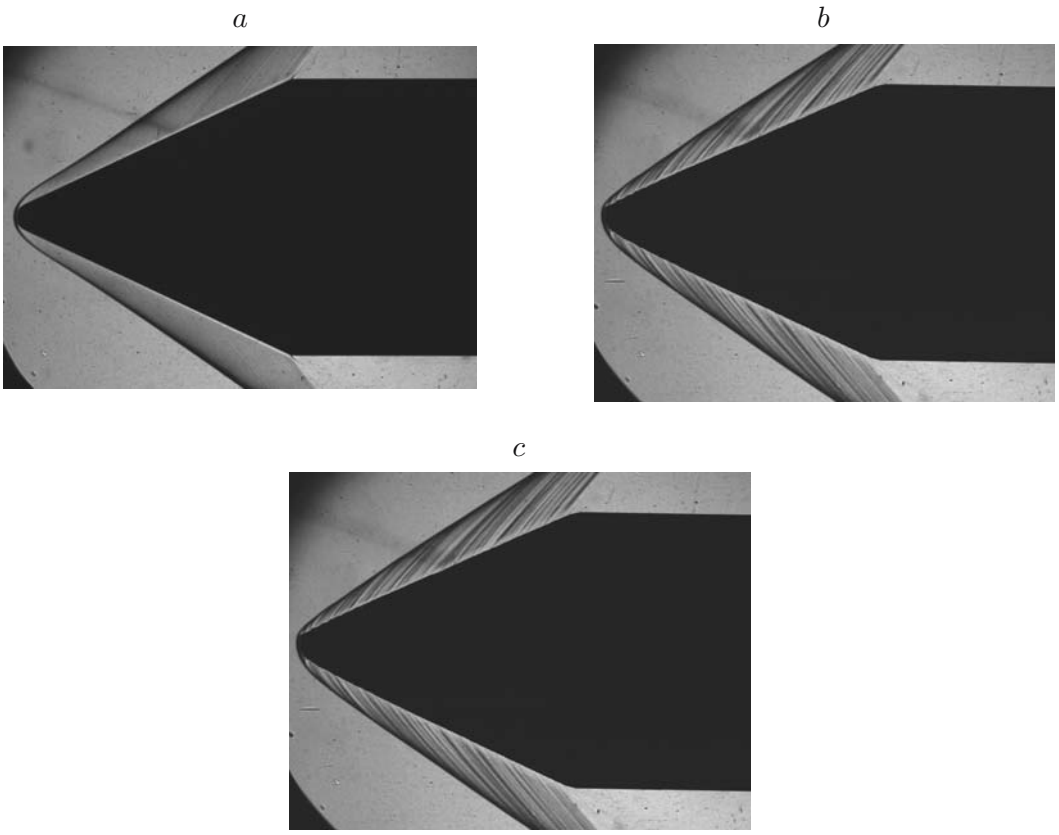

Fig. 8. Schlieren pictures of the flow around the nose cones of different types in a flow with M = 3.02: (a) smooth impermeable cone; (b) porous cone without duct flow; (c) porous cone with duct flow.

Experiments on the Short Model. The experiments on the short model were performed to visualize the flow on the head part of the model with the IAB-451 shadowgraph and to determine the influence of different types of the nose cone on the streamwise static stability. The nose cones described above were used. The air flow through the model body was ensured through holes in the base surface, which could be opened or closed. The total relative area of the holes was $S_{\text{hole}}/S_{\text{mid}} = 14\%$.

The tests were performed at α from -2° to $+10^\circ$ and M = 3.02 and 4.03.

Figure 8 shows the schlieren pictures of the flow with M = 3.02 around different types of the cones (the air mass flow is approximately the same as that indicated above and is equal to $\bar{G} = 1.15\%$).

It was found that the shock-wave structures around the cones are different. In contrast to the smooth cone with a motionless shock-wave front, the pattern around the porous cone contains low-frequency oscillations (waviness) of the shock-wave front: the shock wave is "breathing."

Apparently, the unsteadiness of the bow shock wave is caused by oscillations of the air mass flow, when the mass flow of the gas entering the hollow body at a given time is not equal to the mass flow of the gas exhausting through the pores of the nose cone. This effect was noted in numerical calculations performed in the present work and also in [4].

Figure 9 shows the angles of inclination of the conical shock waves versus the angle of attack α for the windward (β_1) and leeward (β_2) sides of the cone in the flow with M = 3.02. For $\alpha = 0^\circ$ ($\beta_1 = \beta_2$), the angle of wave inclination for the permeable cone with duct flow ($\beta_1 = \beta_2 = 34^\circ$) is smaller than that for the impermeable cone and the permeable cone without duct flow ($\beta_1 = \beta_2 = 35^\circ$).

As the angle of attack is increased to $\alpha = 8$–10°, the angle of wave inclination on the leeward side β_2 for the porous cone, both with and without duct flow, decreases slower than that for the impermeable cone. Apparently, it is caused by air overflow through the permeable surface of the cone from the windward side to the leeward side and testifies that the effective shape of the body is distorted by installation of inserts made of a porous material (see

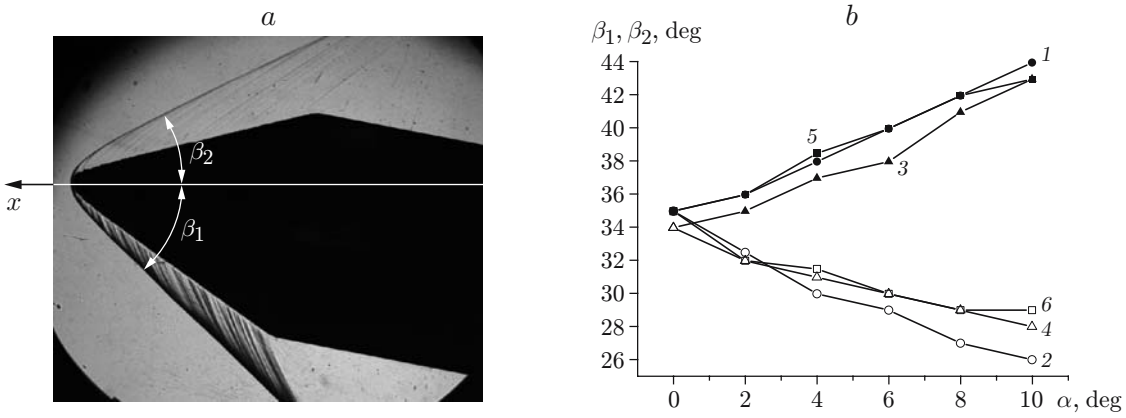

Fig. 9. Schlieren picture of the shock-wave structure around the cone (a) and dependence of the angle of inclination of the bow shock wave on the angle of attack α (b) for the windward β_1 (curves 1, 3, and 5) and leeward β_2 (curves 2, 4, and 6) sides of the cone in a flow with M = 3.02: smooth impermeable cone (1 and 2), porous cone with duct flow (3 and 4), and porous cone without duct flow (5 and 6).

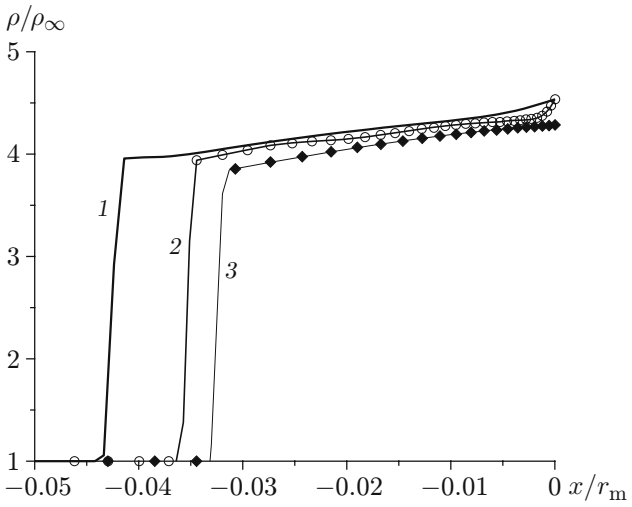

Fig. 10

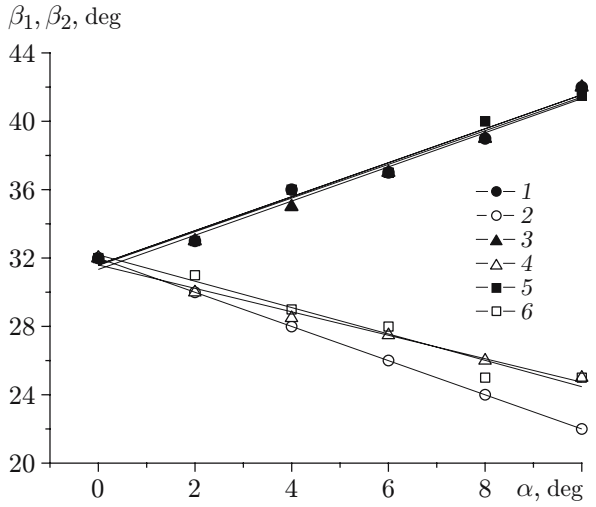

Fig. 11

Fig. 10. Position of the shock wave on the line of symmetry of the body in a flow with M = 3.02 and different relative mass flows of air through the body: $\bar{G} = 0$ (1), 2.6 (2), and 3.8% (3).

Fig. 11. Angles of inclination of the bow shock wave versus the angle of attack α for the windward β_1 and leeward β_2 sides of the cone in a flow with M = 4.03 (notation the same as in Fig. 9).

also [3]). On the windward side at $\alpha \leqslant 8°$, the angles of wave inclination are almost identical for the impermeable surface and the permeable surface without duct flow, whereas the angle of wave inclination for the porous surface with duct flow is smaller by 1–2°. At $\alpha = 10°$, the angle of wave inclination β_1 for the porous surface without duct flow to the base region decreases, which evidences that the intensity of the duct flow through the porous cone increases.

Figure 10 shows the results of the calculated stand-off distance of the shock wave on the line of symmetry of the body for different mass flows of air through the model body in the flow with the Mach number M = 3, which give indirect evidence for experimental data.

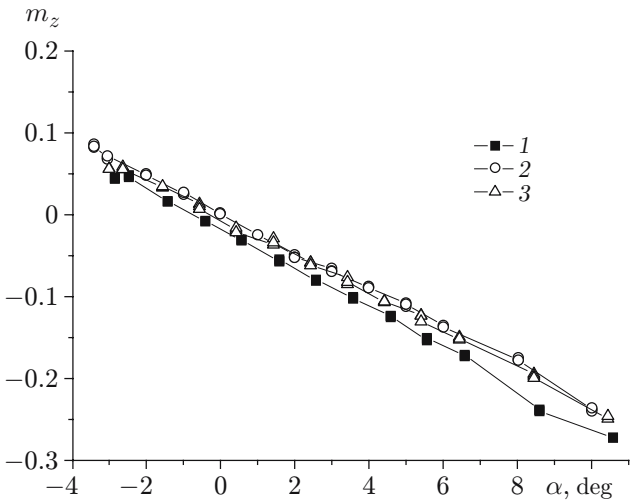

Fig. 12. Pitching moment coefficient m_z versus the angle of attack α in a flow with M = 3.02 for different nose cones ($l_{\text{mod}} = 230$ mm): 1) smooth impermeable cone; 2) porous cone without duct flow; 3) porous cone with duct flow.

As the angle of attack α is increased, the flow with the Mach number M = 4.03 also displays a comparative decrease in the angle of wave inclination on the leeward side of the porous cone, as compared with the impermeable cone (Fig. 11). At $\alpha \geqslant 0°$, the angles of wave inclination on the windward side of the cone are almost identical for all types of cones.

An analysis of the dependence $c_x = f(\alpha)$ in the case of the porous cone with duct flow (see Fig. 4) testifies that it is necessary to study the characteristics of the streamwise stability of the body in more detail, i.e., to study the behavior of the pitching moment m_z.

The coefficient m_z was calculated with respect to the center of gravity conventionally assumed to be located in the apex of the nose cone.

Figure 12 shows the dependence $m_z = f(\alpha)$ for the short model ($l_{\text{mod}} = 230$ mm) in the flow with the Mach number M = 3.02. The slope of the curves, i.e., the value of the derivative $dm_z/d\alpha < 0$, characterizes the degree of the streamwise static stability [13]. It is seen that the slope in the case of the impermeable cone is greater than that in the case of the gas-permeable cone, i.e., the use of the permeable cone reduces the streamwise static stability.

Conclusions. The aerodynamic characteristics of a body of revolution equipped with a porous gas-permeable nose part with an internal duct flow through the body toward the base region in a supersonic flow are studied experimentally and numerically. It is shown that the use of porous inserts decreases the drag coefficient in the flow with the Mach number M = 3.02 approximately by 9% and alters the characteristics of the streamwise static stability. The experimental and numerical results are in good qualitative and quantitative agreement.

REFERENCES

1. N. Frink, D. Bonhaus, V. Vatsa, et al., "A boundary condition for simulation of flow over porous surfaces," in: *Proc. of the 19th Applied Aerodynamics Conf.* (Anaheim, June 11–14, 2001), AIAA, Hampton (2001), pp. 2001–2412.
2. T. Hartman and J. M. Morgenstern, "Passive aerodynamic sonic boom suppression for supersonic aircraft," USA Patent No. 2004/0065774 A1 USA, Publ. 04.08.04.
3. V. N. Zaikovskii, V. P. Kiselev, S. P. Kiselev, et al., "Effect of a porous insert in the supersonic part of the nozzle in changes in the nozzle thrust," *Dokl. Ross. Akad. Nauk*, **401**, No. 4, 479–482 (2005).
4. N. I. Sidnyaev, "Review of methods for studying hypersonic gas flows past bodies with ablative coatings," *Thermophys. Aeromech.*, **11**, No. 4, 489–508 (2004).
5. A. I. Shvets and I. T. Shvets, *Near-Wake Gas Dynamics* [in Russian], Naukova Dumka, Kiev (1976).

6. J. E. Bowman and W. A. Clayden, "Cylindrical afterbodies in supersonic flow with gas ejection," *AIAA J.*, **5**, No. 8, 1524–1525 (1967).
7. D. M. Sykes, "Cylindrical and boat-tailed afterbodies in transonic flow with gas ejection," *AIAA J.*, **8**, No. 3, 588–590 (1970).
8. V. F. Zakharchenko and Yu. Kh. Kardanov, "Base pressure of bodies of revolution with gas ejection through the body surface into a supersonic flow," *Izv. Akad. Nauk SSSR, Mekh. Zhidk. Gaza*, No. 3, 163–167 (1983).
9. G. L. Grozdovskii, Yu. A. Lashkov, G. P. Svishchev, and I. N. Sokolova, "Effect of perforated inserts with streamwise slots on base pressure of a body of revolution at supersonic velocities," *Uch. Zap. TsAGI*, **3**, No. 2, 21–26 (1972).
10. R. A. Yusupov, A. I. Kirdyashkin, and Yu. M. Maksimov, "Laws of SHS of porous composite ceramics and metal ceramics," *Gorenie Plasmokhimiya*, **1**, No. 3, 351–356 (2004).
11. A. V. Lokotko, "Device for aerodynamic tests," Inventor's Certificate No. 1091703, MKI G 01 M 9/00, No. 3479000/40-23, Publ. 05.10.95, Bul. No. 13, Priority 08.05.82.
12. P. Chang, *Separation of Flow*, Pergamon Press, Oxford (1970).
13. N. F. Krasnov, *Aerodynamics of Bodies of Revolution* [in Russian], Mashinostroenie, Moscow (1964).